PCCP

Chemical and Electronic Structures of Cobalt Oxynitride Films Deposited by NH3 vs. N2 Plasma: Theory vs. Experiment

Journal:	*Physical Chemistry Chemical Physics*
Manuscript ID	CP-ART-08-2020-004168.R2
Article Type:	Paper
Date Submitted by the Author:	16-Oct-2020
Complete List of Authors:	Osonkie, Adaeze; University of North Texas, chemistry Lee, Veronica; University of North Texas, chemistry Oyelade, Adeola; University of North Texas, chemistry Mrozek-McCourt, Maximillian; University of North Texas, chemistry Chukwunenye, Precious; University of North Texas, chemistry Golden, Teresa; University of North Texas, chemistry Cundari, Thomas R.; University of North Texas Kelber, Jeffry; University of North Texas, Department of Chemistry

Chemical and Electronic Structures of Cobalt Oxynitride Films Deposited by NH₃ vs. N₂ Plasma: Theory vs. Experiment

Adaeze Osonkie[a], Veronica Lee[a], Adeola Oyelade, Maximillian Mrozek-McCourt[b], Precious Chukwunenye[a], Teresa D. Golden[a], Thomas R. Cundari[a], Jeffry A. Kelber[a]

The chemical structures of Co oxynitrides – in particular, interactions among N and O atoms bonded to the same cobalt – are of great importance for an array of catalytic and materials applications. X-ray diffraction (XRD), core and valence band X-ray photoelectron spectroscopy (XPS) and plane wave density functional theory (DFT) calculations are used to probe chemical and electronic interactions of nitrogen-rich $CoO_{1-x}N_x$ (x > 0.7) films deposited on Si(100) using NH₃ or N₂ plasma-based sputter deposition or surface nitridation. Total energy calculations indicate that the zincblende (ZB) structure is energetically favored over the rocksalt (RS) structure for x > ~ 0.2, with an energy minimum observed in the ZB structure for x ~ 0.8 - 0.9. This is in close agreement with XPS-derived film compositions when corrected for surface oxide/hydroxide layers. XRD data indicate that films deposited on Si (100) at room temperature display either a preferred (220) orientation or no diffraction pattern, and are consistent with either rocksalt (RS) or zincblende (ZB) structure. Comparison between experimental and calculated X-ray excited valence band densities of states – also similar for all films synthesized herein – demonstrates a close agreement with a ZB, but not an RS structure. Core level XPS spectra exhibit systematic differences between films deposited in NH₃ vs N₂ plasma environments. Films deposited by N₂ plasma magnetron sputtering exhibit greater O content as evidenced by systematic shifts in N 1s binding energies. Excellent agreement with experiment for core level binding energies is obtained for DFT calculations based on the ZB structure, but not for the RS structure. The agreement between theory and experiment demonstrates that these N-rich Co oxynitride films exhibit the ZB structure, and forms the basis of a predictive model for understanding how N and O interactions impact the electronic, magnetic and catalytic properties of these materials.

Introduction

Cobalt nitrides and oxynitrides are of significant interest for their unusual magnetic and electronic properties[1] and for numerous applications, including rare earth-free magnets,[2] Li ion batteries,[3] and photo-,heterogeneous, and electro-catalysis.[4-10] Unlike the early transition metal nitrides, cobalt nitrides or oxynitrides are generally made by non-equilibrium methods, including pulsed laser deposition,[1,11] temperature-programmed reaction,[8] sputter magnetron deposition,[9,12,13] and plasma nitridation of a Co metal surface.[14]. Perhaps for this reason, the surface structures and reaction dynamics of these materials—particularly concerning N and O interactions, are not well understood. Co/N ratios are known to directly impact electronic and magnetic properties.[12,13] In an important publication by Lumey and Dronkowski, it was proposed via both plane-wave and muffin-tin calculations that one could, in principle, control the structural and electronic properties of CoO_xN_y phases by varying the nitrogen-to-oxygen ratio.[15] Previous photoemission studies[11,14] have provided a general understanding of core level spectra, but a specific understanding of how varying N/O

stoichiometry may impact such spectra, or valence band densities of states, is lacking.

Herein, we present experimental XRD, core and valence band photoemission data, and DFT calculations, for films deposited by NH₃ sputter deposition or plasma nitridation, and for films deposited by N₂ or Ar/N₂ plasma sputter deposition. A novel finding of practical significance is that films deposited by either NH₃-based or N₂-based plasma methods exhibit similar XRD and valence band photoemission spectra, but systematic differences in core level N 1s spectra that reflect differences in O content. Specifically, films formed by NH₃- based deposition exhibit observably lower O content, yielding systematic shifts in N 1s binding energies relative to films deposited by N₂ or Ar/N₂ plasma sputter deposition.

The results presented here also provide a detailed comparison of calculated and experimental core and valence band photoemission data. Recent studies of transition metal oxides have demonstrated the importance of such comparisons for interpreting and predicting reactive behavior and other properties.[16,17] Focusing here on N-rich $CoO_{1-x}N_x$ films (x > 0.7), plane-wave DFT calculations show that the core and valence band photoemission data observed are indicative of a ZB structure, and inconsistent with a RS structure. Additionally, these calculations provide a detailed interpretation of N 1s and O 1s

a. Department of Chemistry, University of North Texas, Denton, TX 76203.
b. Biology and Physical Science Department, Passaic County Community College, Paterson, NJ 07505.

core level spectra in terms of N and O chemical bonding interactions when these atoms are bound to the same Co atom. As such, this comparison between theory and experiment provides a predictive framework for understanding the various properties of cobalt and related transition metal oxynitrides in terms of varying N/O stoichiometries.

Methods

Experiment.

Two similar DC magnetron sputter deposition chambers were used to prepare $CoO_{1-x}N_x$ films. These are shown schematically in Supplemental Information (Figs. S1 and S2). Chamber 1 (base pressure 1 x 10^{-7} Torr, Fig. S1) was attached to a UHV/XPS analysis chamber permitting direct sample transfer between deposition and analysis chambers without exposure to ambient. Chamber 1 also contained an inductively coupled plasma source described previously.[18] This chamber was used to prepare films by N_2 or NH_3 sputter deposition from a Co target (99.5%), on Si (100), or, alternatively, to prepare films by NH_3 plasma nitridation of a Co film deposited on Si (100). In each case, film deposition was followed directly by sample transfer under controlled conditions to the analysis chamber (base pressure 3 x 10^{-10} Torr) for core and valence band photoemission studies. Chamber 2 (base pressure 3 x 10^{-8} Torr; Fig. S2) was part of a different vacuum system with capabilities for magnetron sputter deposition, temperature programmed desorption, and Auger electron spectroscopy (AES.) In both chambers, the sputter source was a commercial magnetron gun (Meivac MAK sputter source) housing mounted targets of 1.3 inches diameter. Substrate-target distances were 7 inches and 3 inches for Chambers 1 and 2 respectively. In both chambers, sample deposition occurred at room temperature on chemically etched Si (100) substrates. (In the system attached to the XPS chamber, additional Ar ion sputter cleaning of the sample was also carried out.) The base pressure in both film deposition chambers was ~ 1 x 10^{-8} Torr, indicating corresponding amounts of background impurities, including H_2O. As a result, all the deposited films shown here contain at least small but observable amounts of lattice oxygen, even if the plasma gas was entirely NH_3 or N_2.

$CoO_{1-x}N_x$ films were deposited in Chamber 1 by sputtering of a cobalt target using N_2 plasma at 45 W DC power, 3.5 mTorr N_2 pressure and 30 mins deposition time; or NH_3 plasma deposition using 15 W DC power, 3.5 mTorr NH_3 pressure and 15 mins deposition time at room temperature. Electronic grade NH_3 (anhydrous) and N_2 gases were the reactive gas sources. $CoO_{1-x}N_x$ films were also prepared in this chamber using an NH_3 inductively coupled plasma to nitride the surface of a Co/Si(100) film, in a manner similar to that reported previously.[14] This was done at 25 W DC power and 20 mins Co deposition time at room temperature. The film was annealed for 1 hour and afterwards nitrided by direct exposure of the Co film on Si by NH_3 plasma from the ICP source. Plasma conditions was as follows: 20 W, 40 mTorr NH_3 total pressure and 30 secs total nitridation time. For comparison, a $CoO_{1-x}N_x$ film was deposited on Si(100) in Chamber 2 via magnetron sputter deposition with a Co target in Ar/N_2 (1:4) plasma at room

temperature using 25 W DC power, 3 mTorr total Ar/N_2 pressure and 7 mins total deposition time. In all cases, electronic grade gases were used without further purification. A summary of films deposited under these various conditions, with resulting compositions and film thicknesses, is given in Table S1 (Supplemental Information). In the case of films deposited in Chambers 1 and 2, film thicknesses were estimated from sputtering rates determined from data provided by the manufacturer. Corresponding film compositions, as determined by XPS, are also given in Table S1. Importantly, such compositions include surface oxide/hydroxide layers formed during either the deposition process or sample transfer. "Corrected" compositions, representative of bulk film composition, were obtained on selected films by take-off angle resolved spectra or sputtering to remove surface layers, as discussed in the Results section, and are included in Table S1.

XRD data were acquired using a Rigaku Ultima III X-Ray Diffractometer using a Cu K alpha line source and employing the thin film mode. For XRD measurement, 2Θ was used for the scan axis, the scan method was continuous, and the range setting was absolute.

XPS core and valence band spectra were acquired at room temperature - analyzer aligned with the surface normal. XPS spectra were acquired using a commercial 140 mm mean radius hemispherical analyzer with multi-channelplate detector (Physical Electronics) operated in constant pass energy mode (29.35 eV and 23.5 eV for survey and core level spectra respectively), and with a non-monochromatic Al Kα x-ray source. XPS spectra were analyzed using commercial software as described previously.[19] This chamber was also equipped with an ion gun (Omicron) for Ar ion sputtering/cleaning of sample surfaces. Photoelectron inelastic mean free path (imfp) lengths were calculated through CoN (zinc blende structure), using established methods.[20] The imfp lengths for Co 2p, O 1s, N 1s and valence band (BE ~ 2 eV) photoelectrons were calculated to be 14.4 Å, 17.9 Å, 19.7 Å, and 25.1 Å, respectively.

Experimental photoemission spectra were analyzed by standard methods.[21] Deconvolution of core level spectra employed Gaussian-Lorentzian functions with full-width half maxima of 1.5 and 1.8 for N 1s and O 1s spectra, respectively, based on previous experience with this analyzer under similar experimental conditions.[19]

Calculations.

Plane-wave DFT simulations employed the Vienna Ab-initio Software Package (VASP, version 5.4.4).[22] After tests for convergence of predicted properties (lattice constants, Fermi level energies, core level energies, *etc*.), the following computational parameters were selected: energy cutoff = 500 eV, high precision, ISMEAR = 1 (Methfessel-Paxton method[23]), SIGMA = 0.2 (for geometry optimizations; for single-point density of states (DOS) and core level binding energy calculations, ISMEAR = -5 (tetrahedron method with Blöchl corrections[24]), SIGMA = -0.1 eV). All computations were performed using spin-polarized methods in conjunction with PAW potentials[24] and the PBE functional. Calculations were carried out on a single unit cell. Tests with +U corrections did not yield substantially different predicted geometries (*ca.* ±1% in lattice constants for ZB-CoN and hcp-Co) or binding energy shifts (*e.g.*, for ZB-CoN, the

introduction of +U corrections formulated by Goddard and coworkers[25] shifted the Co 2p core energy by 3.9 eV less tightly bound vs. a shift of 4.1 eV in the same direction for the rock salt polymorph), so for production runs, this correction was not utilized. The K-point mesh for all optimizations of solids was 13x13x13.[26] Calculations indicated that the most stable forms of Co and CoN are the hcp and ZB structures, respectively. For the metal, hcp-Co was compared to fcc-Co. For the nitride, ZB and RS structures were evaluated. Calculated lattice parameters are in good agreement with experiment: hcp-Co: $a = b = 2.495$ (2.5071, expt.) Å, $c = 4.032$ (4.0686, expt.) Å, $\alpha = \beta = 90°$, $\gamma = 120°$ (calcd. and expt.); for ZB-CoN, $a = b = c = 4.215$ (4.297, expt.[27]) Å, $\alpha = \beta = \gamma = 90°$.

For accurate calculation of photoemission core level binding energies (without multiplet splittings of, *e.g.*, the Co 2p level), calculations of final state relaxation energies were included to account for the screening response of valence electrons upon formation of a core hole. This was done using the Janek-Slater (JS) method.[17,28] At optimized solid-state geometries, single point DFT calculations were performed on ZB-CoN, RS-CoN, ZB-CoN$_{0.75}$O$_{0.25}$ and RS-CoN$_{0.75}$O$_{0.25}$. For the calculation of N 1s core energy of ZB-CoN and its oxynitride models, the ICORELEVL = 2 option within VASP was utilized with an appropriate CLZ parameter (0.439 e^-), which indicates the number of excited electrons (CLZ = 0.5 e^- corresponds to the Slater-Janak transition state approximation). The CLZ parameter in VASP was set to 0.439 e^- to reproduce the experimentally determined N 1s binding energy of ZB-CoN, -397.5 eV. Utilizing this same value of CLZ for the optimized structure of ZB-CoN$_{0.75}$O$_{0.25}$ yields a N 1s binding energy of -398.0 eV. The 0.5 eV shift in the N 1s binding energy is commensurate with what has been experimentally measured herein, and reported in the literature.[14]

Results

Total Energy Calculations and XRD data.

Calculated total energy differences between ZB and RS structures for CoO$_{1-x}$N$_x$ films are shown in Fig. 1 as a function of N content. These
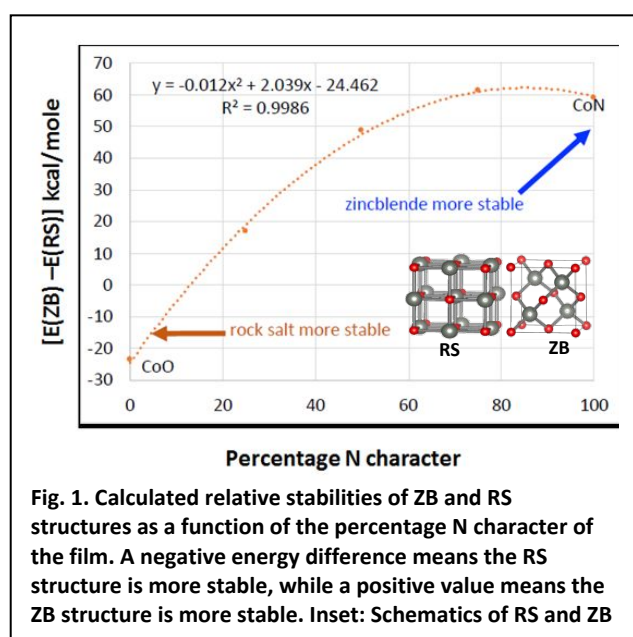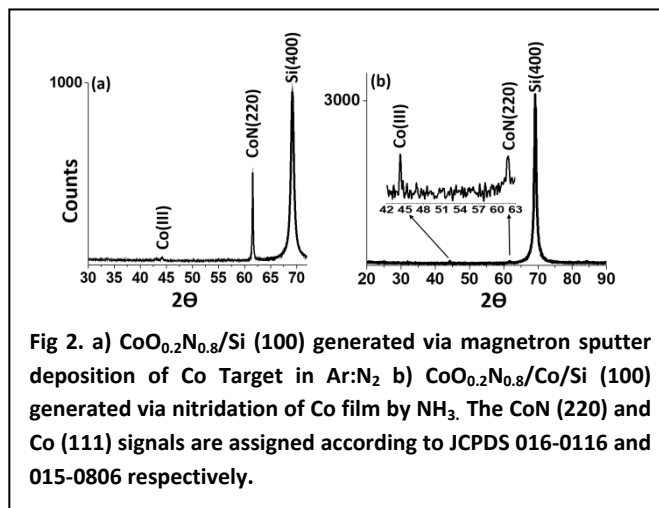

Fig. 1. Calculated relative stabilities of ZB and RS structures as a function of the percentage N character of the film. A negative energy difference means the RS structure is more stable, while a positive value means the ZB structure is more stable. Inset: Schematics of RS and ZB

simulations were performed on solids, which have stoichiometry M$_4$N$_x$O$_{4-x}$ in their unit cells. Different nitrogen and oxygen atom configurations were considered, and the lowest energy structure found among these was chosen. Note that the RS and ZB structures are highly symmetric, so many of these alternate structures gave near identical energies upon optimization. These results indicate that the ZB structure is energetically preferred for N > ~ 0.2. As such, these

Fig 2. a) CoO$_{0.2}$N$_{0.8}$/Si (100) generated via magnetron sputter deposition of Co Target in Ar:N$_2$ b) CoO$_{0.2}$N$_{0.8}$/Co/Si (100) generated via nitridation of Co film by NH$_3$. The CoN (220) and Co (111) signals are assigned according to JCPDS 016-0116 and 015-0806 respectively.

results are consistent with previous calculations for CoO$_{0.5}$N$_{0.5}$ that indicated a ZB structure was energetically preferred for films with equal N and O percentages.[15]

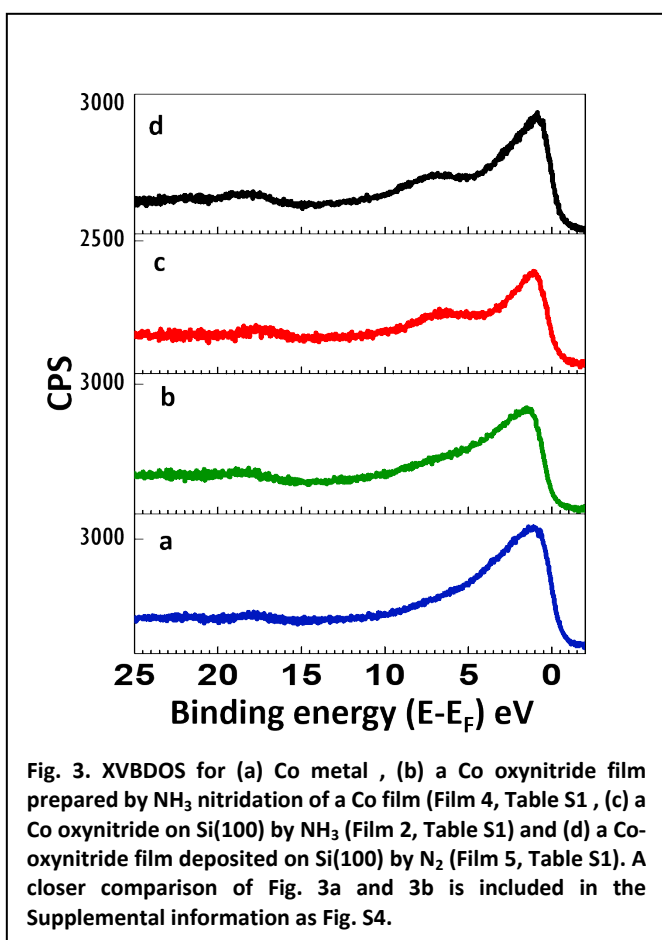These results, however, contrast somewhat with experimental data suggesting insulator-metal transitions and RS-to-ZB phase changes for x > ~ 0.3 and 0.5, respectively [1]. The results in Fig. 1 also indicate that maximum energetic stability for the ZB structure is achieved with non-zero oxygen content, *i.e.*, that a small amount of oxide replacement of nitride in the matrix stabilizes the total energy compared to CoN. As shown below, these predictions are in accord with XPS data for films deposited by pure N$_2$ or NH$_3$, suggesting some driving force for O inclusion, even under highly N-rich and H-rich deposition conditions.

To investigate the crystal structures of N-rich films, XRD spectra were acquired for films deposited by various methods (N$_2$, Ar/N$_2$ or NH$_3$ plasma sputter deposition, NH$_3$ plasma nitridation) onto Si substrates. These films, method of deposition, film composition and XRD data are listed in Table S1. As listed in Table S1, three of the five films examined showed no discernable diffraction pattern, in common with other Co oxynitride films, deposited by PLD.[11] Two films, however, deposited under different plasma conditions and in different chambers, did yield similar diffraction patterns in 2Θ scans, as shown in Fig. 2.
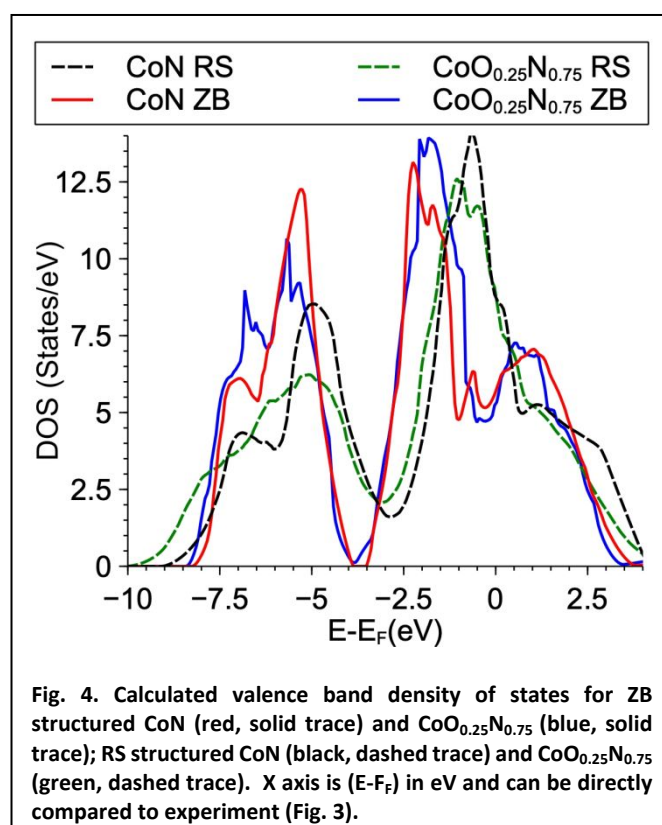
The film deposited on Si (100) at room temperature using Ar:N_2 (1:4) plasma-induced sputter deposition on Si (100) exhibits two non-Si reflections (Fig. 2a), including a weak feature near 2Θ = 44[0] and a more intense feature near 2Θ = 62[0]. Similar, albeit much weaker, features are observed for the second film, formed by NH_3 plasma nitridation of Co. Ex-situ AFM data were acquired for this film (Fig. S3, Supplemental Information), indicating an rms roughness of 1.9 nm. These reflections are identified as Co (111) and CoN (220), respectively.[1,27] The weaker reflections for the film formed by plasma nitridation of Co metal are attributable to a thinner film thickness for the Co oxynitride film formed by this method, consistent with XPS valence band spectra (see below). The observation of a secondary Co metal phase has also been reported for oxynitride films deposited by PLD under different conditions.[1] That two films deposited under different conditions exhibit preferred CoN (220) orientation on Si (100), while others exhibit no diffraction pattern is puzzling, but could be due to those films being amorphous, consistent with other results in the literature.[11] This indicates that deposition factors governing film crystallinity and orientation may depend on certain

CoO_xN_y can be further confirmed using a combination of other techniques[29] not used in this work.

The XRD 2Θ scans are, of themselves, inconclusive in determining the structural phase of the deposited films, as the lack of multiple diffraction peaks prevents the intensity analysis needed to distinguish between RS and ZB structures.[1] The data in Fig. 2 do, however, indicate that deposition on Si(100), under appropriate conditions, leads to a preferred CoN (220) orientation relative to Si (100). The Si (100) in-plane repeat distance for the bulk-terminated lattice is 3.9 Å.[30] The corresponding calculated CoN (220) repeat distance is ~ 4.2 Å for the ZB structure and ~ 4.0 for the RS structure, within 5% of each other. A smaller lattice mismatch occurs for the RS structure, but—especially given the possibility of lattice accommodation at the interface—the observation of preferred (220) lattice orientation cannot be regarded as conclusive in this respect. This is corroborated by previous reports that PLD-deposited Co-oxynitride films of both RS and ZB structure (depending on N content) exhibited epitaxial growth on both MgO(100) (a = 4.2 Å) and on $MgAl_2O_4$(111) (a/2 = 4.0 Å).[1] In summary, in $CoO_{1-x}N_x$ films DFT

Fig. 3. XVBDOS for (a) Co metal , (b) a Co oxynitride film prepared by NH_3 nitridation of a Co film (Film 4, Table S1 , (c) a Co oxynitride on Si(100) by NH_3 (Film 2, Table S1) and (d) a Co-oxynitride film deposited on Si(100) by N_2 (Film 5, Table S1). A closer comparison of Fig. 3a and 3b is included in the Supplemental information as Fig. S4.

Fig. 4. Calculated valence band density of states for ZB structured CoN (red, solid trace) and $CoO_{0.25}N_{0.75}$ (blue, solid trace); RS structured CoN (black, dashed trace) and $CoO_{0.25}N_{0.75}$ (green, dashed trace). X axis is (E-E_F) in eV and can be directly compared to experiment (Fig. 3).

total energy calculations (Fig. 1) decisively favor the ZB structure for $CoO_{1-x}N_x$ for x > ~ 0.8. The XRD data, however, cannot be regarded as decisive in discriminating between ZB and RS structures for the high nitrogen content Co-oxynitride films examined here.

Experimental and Calculated Valence Band data.

Experimental X-ray excited valence band density of states (VBDOS) are shown in Fig. 3 for (a) Co metal, (b) a Co oxynitride film prepared by NH_3 nitridation of a Co film (as in Fig. 2b), (c) a Co

aspects of the deposition process other than those examined here. It is noteworthy to point out that film crystallinity appears to depend on a variety of deposition parameters that are not well understood. It is reasonable to conclude the crystal structure is ZB because it has a hexagonal closed packed structure and we see the Co(111) plane which has the same orientation, however, the crystal structure of

oxynitride on Si(100) by NH_3 (no diffraction peaks), and (d) a Co-oxynitride film deposited on Si(100) by N_2 (no diffraction peaks). (The films in Figs. 3b-d correspond to films numbered 4, 2 and 5, respectively, in Table S1.) The data in Figs. 3a-c demonstrate that the VBDOS undergoes a gradual transition from Co to CoN, with the main peak maximum remaining near 1.0 - 1.5 eV below the Fermi level (E_F), and the growth of a broader secondary shoulder ~ 5 - 8 eV below E_F.

The transitional nature of the film in Fig. 3b, particularly with respect to the evolution the secondary shoulder, is consistent with a relatively thin $CoO_{1-x}N_x$ film formed by plasma nitridation of Co, given that the effective sampling depth for photoelectrons with such energies (~ 2x the imfp) is ~ 50 Å. For the convenience of the reader, a detailed comparison of the spectra in Figs. 3a and b is given in Fig. S4 (Supplemental Information.) This film thickness factor also accounts for the weak XRD features (Fig. 2b). A comparison of the spectra in Figs. 3c and 3d indicates that there is no significant difference in the VBDOS for a film produced by NH_3 vs. N_2 plasma-induced sputter deposition. Calculated VBDOS for ZB and RS CoN and $CoO_{0.25}N_{0.75}$ structures are shown in Fig. 4. For both structures, the addition of a small O component yields only slight shifts in the VBDOS binding energies. The results in Fig. 4, however, demonstrate that the VBDOS for both ZB-structure films exhibit peaks (Co DOS) near 1 - 2 eV binding energy, relative to E_F, and secondary maxima at ~ 5 - 7 eV relative to E_F. These results are in close accord with experimental data for films produced by NH_3 and by N_2 sputter deposition. In contrast, the calculated VBDOS for both RS-structured films (Fig. 4) exhibit
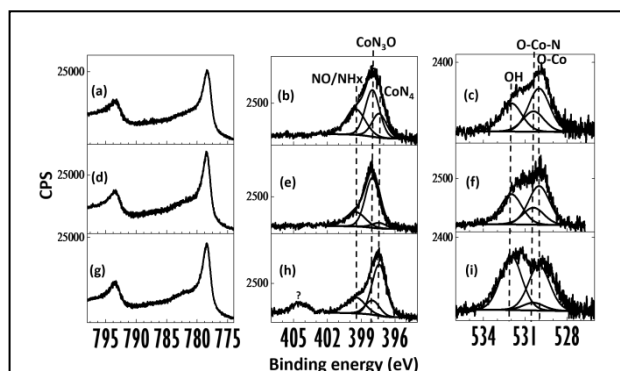

Fig. 5. (a-c) Co 2p, N 1s and O 1s spectra, respectively, for a CoON/Co/Si film produced by NH₃ plasma nitridation of Co/Si; (d-f) corresponding data for a CoON film produced by N₂ plasma sputter deposition; (g-i) corresponding data for a film produced by NH₃ plasma sputter deposition. (These correspond to Films 4, 5, and 2, respectively, Table S1.) Compositions shown are based on data including possible surface oxide/hydroxide layers.

maxima in the DOS at E_F, and secondary DOS maxima at ~ 4 - 6 eV below E_F. Therefore, the calculated results in Fig. 4 show a significantly closer match to experiment (Fig. 3c, d) for films in the ZB, rather than the RS structure.

Experimental Core Level XPS

Core level XPS spectra are shown in Fig. 5 for three different films formed in Chamber 1 and transferred in situ to UHV for XPS analysis. Experimental Co 2p, N 1s and O 1s core level spectra are displayed in

Fig. 5 a-c, respectively, for a film formed by NH_3 plasma nitridation of a Co film deposited on Si (film no. 4, Table S1). The nominal film composition, derived from relative core level intensities acquired in normal emission, and therefore including possible intensities from, *e.g.*, oxide/hydroxide surface layers—is $CoO_{0.2}N_{0.8}$.

Corresponding data are shown in Fig. 5d-f for a $CoO_{0.4}N_{0.6}$ (nominal composition) film formed by N_2 plasma sputter deposition on Si (Film
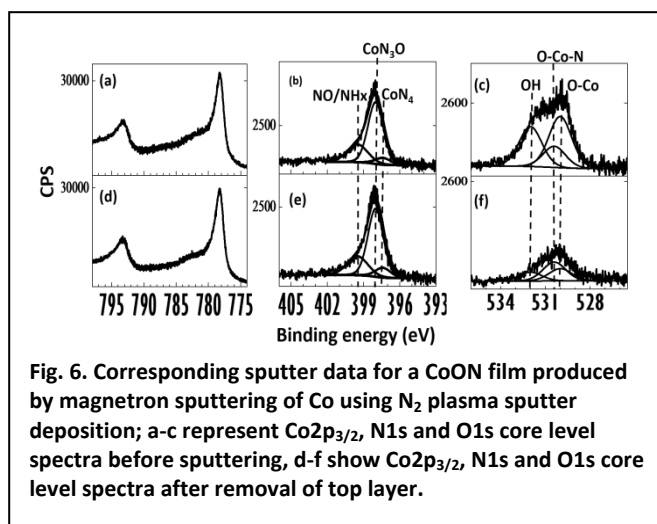

Fig. 6. Corresponding sputter data for a CoON film produced by magnetron sputtering of Co using N₂ plasma sputter deposition; a-c represent Co2p₃/₂, N1s and O1s core level spectra before sputtering, d-f show Co2p₃/₂, N1s and O1s core level spectra after removal of top layer.

no. 5, Table S1), and in Fig. 5h-j for a film formed by NH_3 plasma sputter deposition on Si (nominal composition $CoO_{0.2}N_{0.8}$; film no. 2, Table S1).

As shown in Fig. 5, the Co 2p spectra are similar for all three films, with a single relatively narrow feature at 778.3 eV, in very good agreement with previous results [11, 14]. This binding energy is also characteristic of Co in a +3 oxidation state, as observed for XPS studies of Co_3O_4 films [31, 32].

The N 1s spectra for all three films in Fig. 5 can be deconvoluted into three components centered at binding energies of 397.5 eV, 398.0 eV, and 399.5 eV. The N 1s spectra for the two films formed by NH_3 plasma sputter deposition (Fig. 5b) or NH_3 plasma nitridation (Fig. 5h) are extremely similar in shape, with similar binding energies and nominal film compositions. In contrast, the N 1s spectrum for the film formed by N_2 plasma sputter deposition (Fig. 5e) is shifted to higher binding energy, and also exhibits higher nominal O content than films formed by methods involving NH_3 plasma. As the VBDOS data (Figs. 3 and 4) argue strongly for the ZB structure for these films, the three N 1s components can be tentatively assigned—in order of increasing binding energy—to all N tetrahedra (CoN_4; 397.5 eV), and tetrahedra involving a single O atom ligand (CoN_3O; 398.0 eV), and a higher binding energy component that may represent either NO, in some as yet undetermined bonding environment [14], and/or quite possibly an N-H related feature [33-35]. In view of the low O content of all films synthesized herein, the data argue against peaks arising from multiple O atoms in a tetrahedron about a cobalt atom.

O 1s spectra shown in Fig. 5 are broad and contain at least two major features centered near 530 eV and 532 eV, respectively. Such binding energies correspond closely to those observed for lattice oxygen (530 eV) and surface OH groups (532 eV) for CoO(111) films

formed and analyzed under UHV conditions [32]. The presence of a third feature, attributable to CoN_3O, is certainly possible, but not compelled by comparison with the experimental data (Fig. 5c,f,i). The above assignments, of course, must be regarded as tentative until surface-specific N or O core level features can be distinguished from those more characteristic of the near surface/bulk oxynitride film itself.

Spectra shown in Fig. 6 a-c show Co 2p, N 1s and O 1s spectra respectively, for an oxynitride for a $Co_{0.4}N_{0.6}$/Si film prepared by magnetron sputter deposition of Co using N_2 plasma (the same film as in Fig. 5d-f, Film No. 5, Table S1). Corresponding spectra after Ar ion sputtering are shown in Fig. 7d-f.

The data in Fig.6, acquired at normal emission, show the Co 2p, N 1s and O 1s spectra for this film before and after 1 hr exposure to a 2 keV Ar^+ ion beam (Ar gas pressure at 3.8×10^{-6} Torr, and 4 mA emission current). The data show that this treatment results in no observable change in Co 2p or N 1s spectra, (Fig. 6a,b,d,e) but that sputtering significantly reduces the observed O 1s intensity (Fig. 6 c,f), particularly at binding energies ~ 532 - 533 eV. Thus, no surface-specific states are observed for Co 2p or N 1s spectra, but O 1s states—especially those with binding energies ~ 532 - 533 eV are surface-related. The data in Fig. 6 do, however, also indicate the presence of bulk-related O 1s features at binding energies ~ 530 eV. Based on these results, the film composition after sputtering is estimated at $CoO_{0.2}N_{0.8}$.

In order to test the conclusions regarding surface hydroxyl features, the film prepared by Ar:N_2 plasma magnetron sputter deposition (Film no. 1, Table S1) was subjected to similar Ar ion sputtering to remove the surface oxide/hydroxide layer, and then exposed to H_2O at room temperature to observe reformation of a surface hydroxylated layer. Core level spectra before Ar ion sputtering, after Ar ion sputtering, and after subsequent room temperature exposures to H_2O totalling 10^4 Langmuir, are shown in Fig. 7. Core level spectra before (Fig. 7a-c) and after (Fig. 7d-f) Ar ion sputtering are very similar to corresponding spectra in Fig. 6. Subsequent exposure to 10^4 L H_2O yields no observable change in Co $2p_{3/2}$ or N 1s spectra (Fig. 8g, h), but do yield a significant increase in O 1s spectral intensity near 532 eV binding energy (Fig. 7i). Indeed, after H_2O exposure, the film composition derived from relative N 1s and O 1s intensities is $CoO_{0.4}N_{0.6}$—exactly as observed prior to Ar ion sputtering.

The data in Fig. 7 confirm the assignment of O 1s intensity near 532 eV binding energy as due to a surface hydroxide layer, and also confirm that significant exposure of the sputter-cleaned $CoO_{1-x}N_x$ (N~ 0.8) yields surface hydroxylation with no observable change in Co 2p or N 1s core level spectra. The data in Figs. 6 and 7 also indicate that all films examined here—even those examined immediately upon in situ sample transfer from the deposition chamber—exhibit significant oxide/hydroxide surface layers distinct from the sub-surface "true oxynitride" region. Where possible, film compositions excluding such oxide/hydroxide surface layers are compared to "nominal" compositions incorporating these layers.

The data in Figs. 5 – 7 also corroborate the deconvolution of the N 1s and O 1s experimental spectra as shown in Fig. 5. All films exhibit
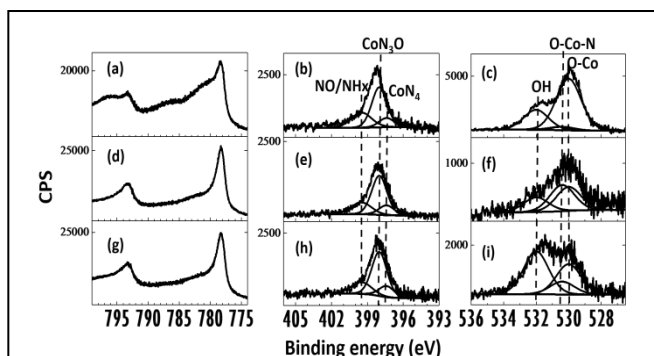

Fig. 7. Core level (a) Co 2p, (b) N 1s and (c) O 1s (spectra of Co oxynitride film produced by magnetron sputtering of Co using Ar/N_2 plasma (Film 1, Table S1),(d-f) corresponding data after subsequent Ar ion sputter cleaning,(g-i) and 10^4L H_2O exposure at room temperature.

a Co $2p_{3/2}$ feature at 778.3 eV. N 1s spectra (Fig. 5) can be deconvoluted into 3 separate N bonding environments as shown in Table 1. Importantly, the data in Figs. 7 and 8 indicate that all N 1s bonding environments observed are characteristic of the bulk structure, rather than specific only to surface states. The N 1s binding energy characteristic of CoN_4 tetrahedra is centered at 397.5 eV, while that characteristic of CoN_3O icosahedra is centered at 398.0 eV. These two assignments explain the shift in N 1s spectra for films prepared by N_2 or Ar/N_2 plasma sputter deposition towards higher binding energies than films prepared by NH_3 plasma sputter deposition or nitridation (Figs. 5 and 7). The films prepared by NH_3-based plasmas all exhibit somewhat lower O content than films prepared by N_2 plasma deposition, even after allowances for surface oxide/hydroxide formation. Therefore, such films exhibit a more intense CoN_4 component (Figs. 5 and 6) than films formed by N_2-based plasma deposition, for which the most prominent feature is that of CoN_3O. The higher binding energy component centered near 399.5 was attributed by Mattson *et al.*[14] to NO formation, as the existence of NO or NO^+ species in plasma-aminated films was confirmed by FTIR. The coexistence of N-H or N-H_2 species, however, cannot be ruled out.[33] Indeed, assigning this feature entirely to N-H or N-H_2 species, exclusive of NO, and then calculating overall film stoichiometries on the basis of relative intensities of the CoN_4 and CoN_3O components yields film compositions close to those provided in Table S1.

Calculated Core Level Binding Energies.

Core level binding energies calculated on the basis of RS or ZB structures, respectively, are compared to experiment in Table 1. Calculated Co $2p_{3/2}$ values are omitted here as such VASP calculations do not resolve the separate spin states.

Table 1 Experimental vs. Calculated Core Level Binding Energies for $CoO_{0.25}N_{0.8}$ and CoO films

Feature	Exp. (eV)	Calc. (ZB) (eV)	Calc.(RS) (eV)

$CoO_{1-x}N_x$			
Co 2p$_{3/2}$	778.3		
N 1s			
CoN$_4$(ZB);CoN$_6$(RS)	397.5	397.5	395.8
CoN$_3$O(ZB); CoN$_5$O(RS)	398.0	398.0	395.9
N-Hx	399.5		
O 1s			
CoN$_3$O(ZB)/CoN$_5$O(RS)	530.0	530.4	529.4
CoO			
Co 2p$_{3/2}$	780.1[1]	NA	
O 1s	530.0[1]	NA	531.0

[1]Experimental values from Olanipekun et al.[32]

The results in Table 1 demonstrate that these calculations produce results in close agreement with experiment for the O 1s spectra of RS-structured CoO. A key point in Table 1 is the difference in N 1s binding energies brought about by common coordination of a single O atom to the same Co atom in the tetrahedron (ZB) or octahedron (RS). The calculated results in Table 1 show a shift of 0.5 eV to higher binding energy in N 1s spectra, precisely in accord with experiment (Fig. 5). In contrast, the introduction of O in the CoN RS lattice results in almost no change in calculated N 1s binding energy (395.8 eV → 395.9 eV, Table 1). Additionally, the calculated O 1s BE in this structure is in close accord with experiment (Figs. 5 - 7), while the calculated O 1s binding energy in the RS structure is too low by ~ 1 eV. In short, the plane-wave DFT calculations accurately model O-Co-N interactions and the subsequent effect upon N 1s binding energies in the ZB structure, but shifts in binding energies are not consistent with the RS structure.

Discussion

A significant issue in the study of Co-oxynitride films is whether the films in question exhibit RS or ZB structure. Ground state total energy calculations (Fig. 1) indicate that the N-rich films examined here should be ZB in nature, in general agreement with previous experimental findings,[1] and theoretical calculations for $CoO_{0.5}N_{0.5}$. What is new about the calculations presented here is the prediction of a local energy minimum for ZB structured $CoO_{1-x}N_x$ films near x ~ 0.8 - 0.9, which is in close agreement to our photoemission-based film stoichiometries once surface oxide/hydroxide layers are excluded. Somewhat surprising, however, is that the XRD data (Fig. 2) show, in some cases, preferred (220) orientation of the deposited cobalt oxynitride film, but in other cases—where broadly similar deposition conditions were employed—no XRD patterns were observed. The latter result is in keeping with those reported for some films deposited by PLD.[11] In contrast, other films deposited by PLD showed extensive diffraction patterns permitting detailed structural analyses over a range of N/O stoichiometries.[1] Clearly, the general method of film growth is not the only determining factor in the overall grain size or other aspects of film structure.

A careful comparison of experimental valence band and core level photoemission spectra with calculations (Figs. 3-5 and Table 1) find consistent agreement with Co-oxynitride models calculated for the ZB structure, but uniform disagreement with results calculated for the RS structure. In summary, although the XRD data are inconclusive, the combination of calculated and experimental photoemission data, and DFT-based energy calculations (Fig. 1) provide a clear indication that the N-rich films examined synthesized herein are ZB in structure.

Results shown in Fig. 5 also demonstrate small but observable and systematic differences for films formed in the presence of NH$_3$ or N$_2$ plasma environments. Films formed in NH$_3$ plasma environments exhibit less O content (excluding surface oxide/hydroxide layers) than films formed in N$_2$ plasma environments. This results in small but systematic shifts in N 1s binding energies.

The finding of lower oxygen content in films formed with NH$_3$ plasma certainly suggests that H reduction of surface O species plays a part in film growth in ammonia environments, and may be of some practical value in fabricating films of especially low O content. Given that other researchers have shown that the catalytic reactivities of transition metal oxynitrides are quite sensitive to the O:N ratio[7,36] this result may have important implications going forward in terms of the reactivity of such films.

The data in Table S1 and in Figs. 6 and 7 also demonstrate that formation of surface oxide/hydroxide overlayers can somewhat distort the apparent O/N atomic ratios in deposited films. The growth of such surface oxide/hydroxide layers as a function of environment is not yet well understood, but the results reported here clearly indicate that some care must be taken when determining Co oxynitride film composition—especially for relatively thin films—whether using in situ or ex suit methods. The results reported here also suggest that the actual surface-specific layers of unsputtered films do not include significant N content. In short, even films transferred in situ from the deposition chamber to UHV exhibit N-free oxide or hydroxide surface layers. These surface layers render films inert towards mild (~10^4 L) exposures to H$_2$O or O$_2$ at room temperature. The presence of such N-free surface layers is also is consistent with detailed studies of TiN oxidation at low-moderate temperatures, indicating that oxidation displaces N atoms from the surface region.[37]

The agreement between experimental and calculated N 1s and O 1s XPS core level binding energies (Table 1) indicates that such calculations, in order to obtain good agreement with experiment, need to include screening relaxation energies in the final state. (Calculations not taking such relaxation into account were far from agreement with experiment and have not been shown here.) This finding is in agreement with calculated core level binding energies for another polar system, LaAlO$_3$/SrTiO$_3$,[17] but differs from those for the less polar Cu-O system.[18] Approaches to calculation of core level binding energies is a topic of long standing interest,[38] but the results reported here suggest that final state relaxation energies in Co-oxynitrides need to be explicitly accounted for.

Summary and Conclusions

$CoO_{1-x}N_x$ films (x > 0.7) were deposited on Si(100) substrates at room temperature by NH$_3$ and N$_2$ magnetron sputter deposition of

Co targets, and by NH_3 plasma nitridation of a Co metal film. XRD measurements indicate that some films exhibit a (220) preferred orientation, while other films exhibited no observable diffraction pattern. Total energy calculations indicate that the ZB structure is preferred for all $CoO_{1-x}N_x$ with x > ~ 0.2, with a local energy minimum for x~ 0.8-0.9, in agreement with film compositions determined by XPS. Comparison of calculated VBDOS and core level binding energies for the ZB structure indicates good agreement with experimental results, while those calculated for the RS structure are inconsistent with experiment. XPS core level spectra also indicate that films produced by NH_3 magnetron sputter deposition on NH_3 nitridation of a Co substrate exhibit observably less O content than films produced by N_2 magnetron sputter deposition. This observation, in concert with calculations, permits identification of specific features in N 1s spectra related to CoN_4 and CoN_3O structures. Going forward, these observations will permit a more detailed understanding of Co-oxynitride composition/reactivity relationships in various environments.

Conflicts of interest

The authors declare no conflict of interest.

Acknowledgements

References

1. J. Takahashi, Y. Hirose, D. Oka, N. Nakao, C. Yang, T. Fukumura, I. Harayama, D. Sekiba and T. Hasegawa, *Appl. Phys. Lett.* 2015, **107**, 231906.
2. X. Zhao, L. Ke, C. Wang and K. Ho, *Phys. Chem. Chem. Phys*. 2016, **18**, 3168-3169.
3. Z. Fu, Y. Wang, X. Yue, S. Zhao and Q.J. Qin, *Phys. Chem. B.* 2004, **108**, 2236-2244.
4. H. Abroshan, P. Bothra, S. Back, A. Kulkarni, J. K. Nørskov and S. Siahrostami, *J. Phys. Chem. C*. 2018, **122**, 4783-4791.
5. Y. Cong, H. S. Park, H. X. Dang, F. F. Fan, A. J. Bard and C. B. Mullins, *Chem. Mater.* 2012, **24**, 579-586.
6. C. Boyadjian and L. Lefferts, *Eur. J. Inorg. Chem*. 2018, 1956-1968.
7. M. L. Kaliya and S. B. Kogan, *Catal. Today.* 2005, **106**, 95-98.
8. Z. Yao, A. Zhu, J. Chen, X. Wang, C. T. Au and C. Shi, *J. Solid State Chem.* 2007, **180**, 2635-2640.
9. M. Azuma, M. Kashihara, Y. Nakato, H. Tsubomura*. J. Electroanal. Chem.* 1988, **250**, 73-82.

10. Y. Yang, R. Zeng, Y. Xiong, F.J. DiSalvo, H.D. Abruña. *J. Am. Chem. Soc.* 2019, **141,** 19241-19245.
11. W. De La Cruz, O. Contreras, G. Soto and E. Pérez-Tijerina, *Rev. Mex. Fis.* 2006, **52**, 409-412.
12. H. Asahara, T. Migita, T. Tanaka, K. Kawabata. *Vacuum.* 2001, **62,** 293-296.
13. R. Gupta, N. Pandey, A. Tayal, M. Gupta. *AIP Adv.* 2015, **5**, 97131-7.
14. E.C. Mattson, D.J. Michalak, W. Cabrera, J.F. Veyan, Y.J. Chabal. Initial nitride formation during plasma nitridation of cobalt surfaces. *Appl. Phys. Lett.* 2016, **109**, 091602.
15. M. W. Lumey and R. Dronskowski. *Adv. Funct. Mater.* 2004, **14**, 371-376.
16. Q. T. Trinh, K. Bhola, P. N. Amaniampong, F. Jerome and S. H. Mushrif, *J. Phys. Chem. C.* 2018, **122**, 22397–22406.
17. I. Fongkaew, R. Akrobetu, A. Sehirlioglu, A. Voevodin, S. Limpijumnong, W.R.L. Lambrecht. J. Electron Spectrosc. Relat. Phenom. 2017, **218**, 21-29.
18. B. Dong, E. Echeverria, A. Oyelade, D. Converse, J. Silva, J.M. Rimsza, J. Du, M.S. Driver, B. Hayworth, N. Shao, Y. Gao, W. Mei, P.A. Dowben, J.A. Kelber. *J. Electron Spectrosc. Relat. Phenom.* 2018, **233,** 21-28.
19. A. Oyelade, A. J. Yost, N. Benker, B. Dong, S. Knight, M. Schubert, P. A. Dowben and J. A. Kelber, *Langmuir*. 2018, **34**, 12007-12016.
20. S. Tanuma, C. J. Powell and D. R. Penn, *Surf. Interface Anal.* 2003, **35**, 268-275.
21. D. Briggs, M.P. Seah. "Practical surface analysis, second edition, volume 1-- auger and X-ray photoelectron spectroscopy" 1990, **1**, 657.
22. J. Hafner and G. Kresse, Properties of Complex Inorganic Solids. Springer, Boston, MA. 1997.
23. M. Methfessel, A. Paxton. *Phys. Rev. B*. 1989, **40**, 3616-3621.
24. P.E. Blöchl. Projected augmented-wave method. Phys Rev B. 1994, **50**, 17593-17979.
25. J. Beatty, T. Cheng, Y. Cao, M. S. Driver, W. A. Goddard, J. A. Kelber. *J. Phys. Chem. Lett.* 2017*, **8**, 188-192.
26. H.J. Monkhorst, J.D. Pack. Special points for Brillouin-zone integrations. *Phys. Rev. B.* 1976, **13**, 5188.
27. K. Suzuki, T. Kaneko, H. Yoshida, H. Morita and H. Fujimori, *J. Alloys Compd.* 1995*, **224**, 232-236.
28. N. Pueyo Bellafont, F. Viñes, W. Hieringer, F. Illas. J. Comput. Chem. 2017, **38**, 518-522.
29. M. Gupta, Y. Kumar, A. Tayal, N. Pandey, W. Caliebe, J. Stahn. S*N Appl. Sci.* 2019*, **2**, 41
30. Y. Tang, R. Wang, Y. Zhang, B. Xiao, S. Li, P. Du. *RSC Adv*. 2019, **9**, 20345-20355.
31. S.C. Petito, M.A. Langell. *J. Vac. Sci. Technol*. A. 2004, **22**, 1690-1695.
32. O. Olanipekun, C. Ladewig, T. Estrada, J. A. Kelber, M. D. Randle, J. Nathawat, C. Kwan, J. P. Bird, P. Chakraborti, P. A. Dowben, T. Cheng and W. A. Goddard III, *Semicond. Sci. Technol.* 2017, **32**, 095011.
33. C. Fettkenhauer, X. Wang, K. Kailasam, M. Antonietti, D. Dontsova. *J. Mater. Chem. A*. 2015, **3**, 21227-21232.

34. B. Cao, G.M. Veith, J.C. Neuefeind, R.R. Adzic, P.G. Khalifah. *J. Am. Chem. Soc.* 2013, **135**, 19186-19192.
35. H. Liu, H. Zhang, H. Xu, T. Lou, Z. Sui, Y. Zhang. *Ceram. Int.* 2018, **44,** 1583-1588.
36. X. Yang, J. Nash, J. Anibal, M. Dunwell, S. Kattel, E. Stavitski, K. Attenkofer, J.G. Chen, Y. Yan, B. Xu. *J. Am. Chem. Soc.* 2018, **140**, 13387-13391.
37. J. Graciani, J. Fdez Sanz, T. Asaki, K. Nakamura, J.A. Rodriguez. Interaction of oxygen with TiN(001):N↔O exchange and oxidation process. *J*. Chem. *Phys*. 2007, **126**, 244713.
38. P.S. Bagus, F. Illas, G. Pacchioni, F. Parmigiani. J. Electron Spectrosc. Relat. Phenom. 1999, **100**, 215-236.